Chapter 2

Thermodynamics of pure metals and alloys

2.1 Introduction

Crucial to the design and processing of materials is a quantitative understanding of the phase-equilibrium information with respect to constraints such as temperature, pressure and composition. This information is captured graphically in phase or equilibrium diagrams. The determination of phase diagrams has been a largely empirical process. So far, the phase diagrams for most binary alloy systems are known, but only limited information is available for phase diagrams of ternary or higher order systems. The lack of information for higher-order system causes many difficulties in developing alloys such as metallic glasses because much of the work has to be done by trial and error (Peker, 1994). Therefore, it is instructive to consider phase diagrams from a simple thermodynamic point of view so that we can extend our knowledge to the phase behavior of higher order systems.

In considering the general alloy case, each element can be characterized by atomic size, cohesive energy, bulk modulus, and other physical and chemical properties. Among theses, atomic size is known to be the dominant factor in determining the phase-equilibrium properties (Hume-Rothery, 1969). For example, solute solubility in crystalline solids is related to atomic size differences between the solute and solvent atoms and solubility becomes very limited (about 5%) when the atomic size of two metals differ by more than 15% (or 85% size ratio), which is called as the Hume-Rothery

rule. Experimentally, a large number of binary alloys (about 90%) show agreement with this rule (Hume-Rothery, 1969).

In this chapter, we consider a model binary systems with differing atomic size ratios to qualitatively understand its effect on the phase equilibrium behavior. Thermodynamic properties are calculated using molecular dynamics (MD) simulations. Conventional empirical relations are initially employed to describe the thermodynamic functions of pure metals. Then, a simple model is proposed to describe the thermodynamic properties of alloys as a function of alloy composition. In particular, the excess vibrational entropy of solid solution is calculated using the elastic constants of the system. Using this model, the polymorphic melting line $T_0(x)$ is determined. In alloys with fixed composition, the polymorphic melting temperature decreases as the size ratio decreases. Especially at the size ratio 0.85, $T_0(x)$ plunge sharply and crosses the glass transition line $T_g(x)$, which is a favorable condition for the glass formation according to the T_0 criterion of glass formation (Massalski, 1981).

2.2 Simulation methods

We use generalized binary alloy systems which are composed of atoms of different sizes (Cu^* and Cu^{**}). The size ratio l is defined as the ratio of size of Cu^* atom to size of Cu^{**} atom (see Chapter 3). The l value used in this study is 0.85, which is considered to be a critical size ratio for the solubility of a solid solution (Hume-Rothery, 1969). This study is then extended to systems of different atomic size ratios.

To simulate Cu binary alloys, the Sutton-Chen (SC) type many-body force field was used (Sutton and Chen, 1990; Rafiitabar and Sutton, 1991). The force-field

parameters for theses systems are summarized in Table 2-1. As shown in the Table 2-1, we changed only the lattice parameter while keeping other parameters constant. Therefore, theses simulations only differ in the atomic size ratio and excess chemical effects are minimized.

The MD simulations were performed using systems with 500 atoms per periodic cell (single phase simulation). To obtain thermodynamic data of solid and liquid phases at various temperatures, heating and cooling simulations are performed using *TtN* (constant temperature and constant stress) dynamics (Ray and Rahman, 1985). During a heating simulation, a random FCC solid solution is raised from 100K to couple of hundred degrees above the melting temperature in increments of 100K for 25ps, which leads to a heating rate of 4×10^{12} K/s. After the sample reaches an equilibrium liquid state, a cooling simulation is carried out to 100 K, again in decrements of 100K for 25ps.

Since MD with a high heating rate and PBC (no interface) results in the superheating of crystals, the equilibrium melting temperature T_m is determined using two phase simulations. A two phase simulation is performed by combining equilibrium liquid (N=1000) and crystal (N=1000) atoms together in one cell under *TtN* conditions. For example, the two phase simulation for the pure Cu^{**} system is shown in Fig. 2-1(a) and (b). At $T<T_m$, the portion in the crystalline state increases as the simulation time t increases due to the crystallization of the liquid phase. For the same reason, the enthalpy H of the total system decreases until the system reaches an equilibrium state, which is the crystalline state in this case. Conversely, at $T>T_m$, the portion of the liquid state increases with the simulation time t. Therefore, the H of the total system increases until the system becomes completely the liquid state. At $T=T_m$, the sample remains as half liquid and half

crystal, which is the same as the initial state. Therefore, the H of the total system stays constant as a function of t at $T=T_m$. For pure Cu* and Cu**, the melting temperature obtained from the single phase simulation is ~1300K but the equilibrium melting temperature T_m from two phase simulation is ~1100K. Therefore, ~18% superheating was achieved in the single phase simulation with a heating rate of 4×10^{12} K/s, which agrees with the prediction based on homogeneous nucleation theory (Luo and Ahrens, 2003).

In addition to the simple thermodynamic properties, the elastic constants C_{ij} of the solid solutions were measured. The elastic constants were calculated by averaging the statistical fluctuations for 25ps using *EhN* (constant energy and shape) dynamics. Thus, the obtained elastic constants contain the Born term (Born, 1954) as well as contributions from the microscopic stress fluctuation and kinetic energy (Cagin and Ray, 1988a, d, b, c).

2.3 Thermodynamic properties of pure metals

Above room temperature, the temperature dependence of the heat capacities (solid and liquid) can be described by an empirical equation, such as

$$C_p(T) = A + BT + CT^2 + \frac{D}{T^2}. \qquad (2\text{-}1)$$

Here, A, B, C, and D are empirical constants and values for various substances can be found in references (J. M. Smith, 1987; O. Kubaschewski, 1993).

Subsequently, the enthalpy H and the entropy S can be obtained as:

$$H(T) = \int C_p(T)dT = AT + \frac{B}{2}T^2 + \frac{C}{3}T^3 - \frac{D}{T} + E, \qquad (2\text{-}2)$$

$$S(T) = \int \frac{C_p(T)}{T} dT = A \ln T + BT + \frac{C}{2} T^2 - \frac{D}{2} \frac{1}{T^2} + F \,, \qquad (2\text{-}3)$$

where, E and F are constants.

Since the enthalpy can be easily measured using MD simulations, the constants A, B, C, D, and E of Eq. 2-2 for model FCC solid and liquid systems can be obtained by data fitting (Fig. 2-2). Using this method, the constants for FCC solids are found to be A^X=0.0329042kJ/mol/K, B^X=-1.88217×10^{-5}kJ/mol/K^2, C^X=1.92954×10^{-8}kJ/mol/K^3, D^X=-228.536kJK/mol, and E^X=-341.721kJ/mol. And the constants for liquids are found to be A^L=0.0469092kJ/mol/K, B^L=-1.49059×10^{-5}kJ/mol/K^2, C^L=3.97697×10^{-9}kJ/mol/K^3, D^L=453.934kJK/mol, and E^L=-341.002kJ/mol. Here, the superscript X and L represent crystal and liquid, respectively. In addition, the heat capacities of the crystal and liquid states are obtained from Eq. 2-1 using the constants obtained from Eq. 2-2 and the result is shown in Fig. 2-3. Near room temperature, the heat capacity of a crystal ($C_p{}^X$) is approximately 27J/mol/K, which agrees with the Dulong-Petit rule ($C_p{}^X \sim 26.942$J/mol/K) (Swalin, 1972). And at $T \sim T_m$, the Turnbull approximation ($C_p{}^X \sim C_p{}^L$ at T~T$_m$) is also valid (Turnbull, 1950).

For convenience, the differences of the thermodynamic properties between liquids and solids can be defined as:

$$\Delta H^{LX}(T) = H^L(T) - H^X(T) = a \cdot T + \frac{b}{2} \cdot T^2 + \frac{c}{3} \cdot T^3 - \frac{d}{T} + e \,, \qquad (2\text{-}4)$$

$$\Delta C_p^{LX}(T) = C_p^L(T) - C_p^X(T) = a + bT + cT^2 + \frac{d}{T^2}, \text{ and} \qquad (2\text{-}5)$$

$$\Delta S^{LX}(T) = S^L(T) - S^X(T) = \Delta S^{LX}(T_m) + a \cdot \ln(\frac{T}{T_m}) + b \cdot (T - T_m) + \frac{c}{2} \cdot (T^2 - T_m^2) - \frac{d}{2} \cdot (\frac{1}{T^2} - \frac{1}{T_m^2}) \,, \qquad (2\text{-}6)$$

where $a = A^L - A^X$, $b = B^L - B^X$, $c = C^L - C^X$, $d = D^L - D^X$, $e = E^L - E^X$. The first term in Eq. 2-6 can be obtained using the relationship

$$\Delta S^{LX}(T_m) = \frac{\Delta H^{LX}(T_m)}{T_m}. \quad (2\text{-}7)$$

The calculated entropy of fusion $\Delta S^{LX}(T_m)$ from MD simulations is 10.175±0.1J/mol/K, which agrees with the Richard's rule for FCC metals (Gordon, 1983). $\Delta H^{LX}(T)$ and $\Delta S^{LX}(T)$ are shown in Fig. 2-4. The temperature at which $\Delta S^{LX}=0$ is the Kauzmann temperature T_k (Kauzmann, 1948) and T_k is the lower bound for crystallization or the glass transition. From Fig. 2-4, T_k is found to be 413 K, which is $0.38T_m$. There is no experimental T_k data available for pure metals, but theoretically it is predicted to be approximately $0.3T_m$~$0.4T_m$ (Mezard and Parisi, 2000).

2.4 Thermodynamic properties of alloys

Consider the $Cu^{*}_{1-x}Cu^{**}_{x}$ model binary alloy system with l=0.85. The enthalpy H of random FCC solid solutions and the enthalpy of liquid mixtures are shown in Fig. 2-5(a) and (b), respectively. We assume that the enthalpy of mixing (or excess enthalpy) can be described by a parabolic equation, such as the regular solution model (J. M. Prausnitz, 1986).

$$\Delta H^{mix}(x,T) = \Omega x(1-x) \quad (2\text{-}8)$$

Here, x is a mole fraction of Cu^{**} and Ω is an empirical constant. As shown in Fig. 2-5, this provides an excellent description of the enthalpy of mixing in both solid and liquid states. As a result, the enthalpy of random FCC solid solutions can be expresses as

$$H^X(x,T) = H^X(0,T) + \Omega^X x(1-x), \quad (2\text{-}9)$$

and the enthalpy of liquid mixtures can be expressed as

$$H^L(x,T) = H^L(0,T) + \Omega^L x(1-x). \quad (2\text{-}10)$$

Here, the *H(0,T)* term represents the enthalpy of the pure system. Note that *H(0,T)=H(1,T)* because pure Cu* and Cu** have the same thermodynamic properties.

The calculated Ω values at different temperatures are shown in Fig. 2-6. Ω^L seems independent of temperature; however, Ω^X shows a strong temperature dependence. Therefore, we assume that Ω^L is constant as 5.38938 kJ/mol and Ω^X is a linear function of T:

$$\Omega^X(T) = a^X T + b^X, \quad (2\text{-}11)$$

where, a^X=0.0134455kJ/mol/K and b^X=24.6167kJ/mol. Subsequently, the difference in enthalpy, heat capacity, and entropy between liquids and solids are derived:

$$\Delta H^{LX}(x,T) = \Delta H^{LX}(0,T) + (\Omega^L - a^X T - b^X)x(1-x), \quad (2\text{-}12)$$

$$\Delta C_p^{LX}(x,T) = \Delta C_p^{LX}(0,T) + (-a^X)x(1-x), \quad (2\text{-}13)$$

$$\Delta S^{LX}(x,T) = \int \frac{\Delta C_p^{LX}(x,T)}{T} dT = \Delta S^{LX}(0,T) + (-a^X)x(1-x)\ln T + f(x), \quad (2\text{-}14)$$

where, $f(0) = f(1) = 0.0$. The measured $\Delta H^{LX}(x,T)$ MD data and Eq. 2-12 are plotted together in Figure 2-7 and show good agreement.

Consider now $\Delta S^{LX}(x,T)$. The functional form of $\Delta S^{LX}(x,T)$ in Eq. 2-14 contains the unknown term *f(x)*. Since *f(x)* should be symmetric around x=0.5 and the boundary conditions are $f(0) = f(1) = 0.0$, the form $f(x) = gx(1-x)$ can be assumed, where g is a constant. Then, Eq. 2-14 can be rewritten

$$\Delta S^{LX}(x,T) = \Delta S^{LX}(0,T) + (g - a^X \ln T)x(1-x). \quad (2\text{-}15)$$

Now, using $\Delta H^{LX}(x,T)$ and $\Delta S^{LX}(x,T)$, the Gibbs free energy difference between the liquid and solid can be derived as

$$\Delta G^{LX}(x,T) = \Delta H^{LX}(x,T) - T\Delta S^{LX}(x,T). \quad (2\text{-}16)$$

Since $\Delta G^{LX}(x)=0$ at the polymorphic melting temperature $T_0(x)$, the parameter g can be determined if $T_0(x)$ is known. For this purpose, the two phase simulation is carried out to obtain T_0 at x=0.5. It is reasonable to use the two phase simulation method to find $T_0(x)$ because the two phase simulation prohibits long range diffusion between the liquid and solid phases due to its geometric confinement (Fig. 2-1(a)). At x=0.5, we obtain T_0<500K. However, further simulation is impossible because the liquid phase becomes a glass at T<500K. Subsequently, the additional points x=0.4 and x=0.6 are tried to determine T_0. Again, the situation $T_0 < T_g$ is encountered. Finally, the points x=0.3 and x=0.7 are tried and T_0=650K±50K is found. From this result, g is determined to be 72.9 J/mol/K. Using this value, $\Delta S^{LX}(x,T)$ and $\Delta G^{LX}(x,T)$ are calculated and shown in Fig. 2-8 and Fig. 2-9, respectively. Also, the polymorphic melting line $T_0(x)$ is calculated and shown in Fig. 2-10. According to the $T_0(x)$ criterion of glass formation, the glass forming zone is the concentration range that satisfies $T_0(x)<T_g(x)$, where $T_g(x)$ is the glass transition temperature line (Baker and Cahn, 1971; Massalski, 1981). This is because, thermodynamically, polymorphic crystallization needs to be avoided to form glasses. Using the measured T_g=500K±50K at x=0.5 and assuming the constant T_g around x=0.5, we find that the glass forming regime is $0.36<x<0.64$ (Fig. 2-10). Since the concentration dependency of T_g is smaller than that of T_0, the constant T_g assumption at around x=0.5 is reasonable, especially in a relatively narrow concentration range.

So far, we have used the simple model to describe the thermodynamic properties of alloy systems and predicted the glass forming region using the T_0 criterion of glass formation. To obtain the complete phase diagram information including solidus, liquidus, and miscibility gaps in different phases, the accurate entropies of each phase are required. Therefore, the entropic properties of alloy phases are studied.

2.4.1 The entropy of solid solutions

In general, the entropy of mixing ΔS^{mix} of solid solutions can be expressed as the sum of four contributions,

$$\Delta S^{mix} = \Delta S_{conf} + \Delta S_{vib} + \Delta S_{mag} + \Delta S_{el}, \quad (2\text{-}17)$$

where ΔS_{conf} is configurational entropy of mixing, ΔS_{vib} is vibrational entropy of mixing, ΔS_{mag} is magnetic entropy of mixing, and ΔS_{el} is electronic entropy of mixing (Swalin, 1972). While the configurational and vibrational contributions are generally important, the magnetic and electronic contributions are present only in a system that contains strong chemical interactions, such as transition metal alloys. In the simple model binary solid solution, where magnetic and electronic contributions can be ignored, ΔS^{mix} is only the sum of ΔS_{conf} and ΔS_{vib}.

First, let's consider the configurational entropy of mixing. ΔS_{conf} is the sum of the ideal and excess configurational entropies of mixing:

$$\Delta S_{conf} = -R\{x\ln(x) + (1-x)\ln(1-x)\} + \Delta S_{conf}^{EX}. \quad (2\text{-}18)$$

The excess term ΔS_{conf}^{EX} is present if the constituent atoms of the mixture differ in size or if the heat of mixing is nonzero. Previously, ΔS_{conf}^{EX} has been described using

thermodynamic properties, such as the atomic volume, the thermal expansion coefficient, and the isothermal compressibility (Sommer *et al.*, 2001). However, this model assumed that the coordination number is infinite, which is clearly not true for the crystalline materials. As of yet, there has been no direct comparison between this model and experiments to validate the model for crystalline materials.

The vibrational entropy can be derived using Einstein's formula at above the Debye temperature q_D. In this temperature range, most vibrational frequencies are close to the Debye frequency w_D. Therefore, the vibrational entropy S_{vib} per mole is

$$S_{vib} = 3R\left(\ln\frac{k_B T}{\hbar w_D} + 1\right), \tag{2-19}$$

where, $\hbar = \frac{h}{2p}$ and h is Planck's constant. Consider now an alloy formation $xA + (1-x)B \rightarrow C$. If w_A, w_B, and w_C are the Debye frequency of pure A, pure B and pure C, respectively, the change in vibrational entropy due to the alloy formation can be expressed as

$$\Delta S_{vib} = 3R\ln\frac{w_A^x \cdot w_B^{(1-x)}}{w_C}. \tag{2-20}$$

The Debye frequency w_D is only a function of the velocity of sound in the solid and on the number of atoms N per unit volume V,

$$w_D = c_S\left(6p^2\frac{N}{V}\right)^{1/3}, \tag{2-21}$$

where c_S is the effective sound velocity defined by

$$\frac{3}{c_S^3} \equiv \frac{1}{c_L^3} + \frac{2}{c_T^3}. \tag{2-22}$$

Note that c_S reduces simply to the velocity of sound if the longitudinal sound velodity c_L is equal to the transverse sound velocity c_T. Further, c_L and c_T can be expressed in terms of the elastic constants of the medium by the relations:

$$c_L = \left(\frac{G^L}{r}\right)^{1/2} \text{ and } c_T = \left(\frac{G^T}{r}\right)^{1/2}, \tag{2-23}$$

where r is the density of the medium, G^L is the effective elastic constant in the longitudinal mode and G^T is the effective elastic constant in the transverse mode.

With the exception of isotropic materials (where $C_{44} = \frac{1}{2}(C_{11} - C_{12})$), G^L and G^T vary according to the direction of the elastic waves in the system. Since no simple expression for G^L and G^T is available for the general wave vector, we use the geometric average of the effective elastic constants in the three principle propagation directions to represent the average effective elastic constants in the cubic crystal. The geometric average of the elastic constants was previously used to find the dependence of the Debye temperature on the elastic constants for cubic crystals and showed a good agreement with experiments (Blackman, 1951; Siethoff and Ahlborn, 1995).

For the three principle propagation directions [100], [110], and [111] in cubic crystals, effective elastic constants are expressed as (Kittel, 1996):

$$G^L_{[100]} = C_{11} \text{ and } G^T_{[100]} = C_{44} \text{ (in the [100] direction)}, \tag{2-26}$$

$$G^L_{[110]} = \frac{1}{2}(C_{11} + C_{12} + 2\cdot C_{44}),\ G^{T1}_{[110]} = C_{44}, \text{ and } G^{T2}_{[110]} = \frac{1}{2}(C_{11} - C_{12}) \tag{2-27}$$

(in the [110] direction),

$$G^L_{[111]} = \frac{1}{3}(C_{11} + 2\cdot C_{12} + 4\cdot C_{44}) \text{ and } G^T_{[111]} = \frac{1}{3}(C_{11} - C_{12} + C_{44}) \tag{2-28}$$

(in the [111] direction).

Then, the effective elastic constants are

$$G^L = \left(G^L_{[100]} G^L_{[110]} G^L_{[111]}\right)^{1/3} \quad \text{and} \tag{2-29}$$

$$G^T = \left(G^T_{[100]} (G^{T1}_{[110]} G^{T2}_{[110]})^{1/2} G^T_{[111]}\right)^{1/3}. \tag{2-30}$$

In Fig. 2-11, the elastic constant is shown as a function of x for binary FCC solid solution. Subsequently, G^L and G^T (Fig. 2-12) and c_T, c_L and c_S (Fig. 2-13) are calculated. Using the calculated c_S and Eq. 2-21, w_D is calculated. In addition, q_D is calculated as a function of x using the relationship $q_D = \frac{\hbar}{k_B} w_D$ (Fig. 2-14). Note that q_D is dependent on the temperature, which is non-physical. We attribute this to the Debye approximation (Reif, 1985), which is used in deriving Eq. 2-21. However, the temperature dependency of q_D is considerably small (40K over 400K simulation temperature range), therefore, we conclude that the Debye approximation is still reasonable for T=300K. Finally, the excess vibrational entropy is calculated using Eq. 2-20 and w_D. As shown in Fig. 2-15, the vibrational entropy of mixing shows very small temperature dependency, which agrees with Eq. 2-20.

2.5 The effect of size ratio on thermodynamic properties

The same procedures as described in the Section 2.3 and 2.4 are performed to determine the thermodynamic properties of alloys with different l. Since H, S, and G of pure metals with l=0.90 and 0.95 are the same as l=0.85, we focus on the thermodynamic properties of alloys. The obtained Ω^X and Ω^L are shown in Fig. 2-16. The Ω^X are fitted to the Eq. 2-11. We find a^X=0.877145J/mol/K and b^X=2.894KJ/mol for

the l=0.95 system and a^X=2.90975J/mol/K and b^X=12.8856kJ/mol/K for the l=0.90 system. Ω^L are fitted to a constant as 0.625923kJ/mol for the system of l=0.95 and 2.32862kJ/mol for the system of l=0.90.

To determine the g for each system, the polymorphic melting temperature at x=0.5 is determined. T_0 at x=0.5 is found to be 1038±13K for l=0.95 and T_0=913±13K for l=0.90. Corresponding g values are 5.0J/mol/K for l=0.95 and 13.0J/mol/K for l=0.90. Subsequently, the $T_0(x)$ lines are obtained and plotted in Fig. 2-17. When compared to Fig.1-3 in Chapter 1, it is clear that the glass forming ability increases as l decreases. Also, the excess vibrational entropy as a function of l and x are calculated using the elastic constant of alloys. We find that the excess vibrational entropy increases as l decreases (Fig. 2-18).

2.6 The Lindermann melting formula and Debye temperature

The Lindemann melting formula describes the melting temperature of the solid as

$$T_m = \frac{r_m^2}{9\hbar^2} M k_B q_D^2 r_S^2, \qquad (2\text{-}31)$$

where M is the atomic mass and r_m is the mean square amplitude of the vibration of each atom divided by the mean radius of a unit cell r_S (Ziman, 1972). In most solids, r_m is in the range of 0.2-0.25. Previously, we obtained the T_m of pure Cu* and Cu** at 1088K. Based on the T_m, q_D can be calculated using Eq. 2-31 if r_S is known. The r_S for pure Cu** is calculated using the atomic volume at T=1088K and found to be 0.247nm. Subsequently, q_D of pure Cu** is calculated and found to be 140K (if r_m=0.25)-170K (if r_m=0.20), which are one half of the q_D calculated using the elastic constants (Fig. 2-14).

Therefore, Eq. 2-31 significantly underestimates q_D. This is because Eq. 2-31 is derived based on the assumption that c_T=c_L, which is not true in this case (Fig. 2-13). The factor 9 in Eq. 2-31 should be modified if c_T is not equal to c_L.

Ignoring the pre-factors in Eq. 2-31 and considering only the material properties,

$$T_m \propto M q_D^2 r_S^2 . \tag{2-32}$$

Because pure Cu* and Cu** have the same melting temperature and atomic mass, Eq. 2-31 can be reduced to

$$q_D \propto \frac{1}{r_S}. \tag{2-33}$$

In addition, r_S is proportional to the lattice constant a (Table 2-1), so Eq. 2-33 can be further reduced to

$$q_D \propto \frac{1}{a}. \tag{2-34}$$

In Fig. 2-19, q_D and $1/a$ are plotted for pure Cu* and Cu** at l=0.85, 0.90, and 0.95. q_D is calculated from the elastic constants at T=300K using the method described in Section 2.4.1. The results show good agreement with Eq. 2-34, giving the correlation constant R^2=0.9987. Therefore, we conclude that the q_D calculated from the elastic constants in this work is reasonably accurate based on the prediction of the Lindemann melting formula.

2.7 Conclusion

The thermodynamic properties of pure metals and alloys are calculated using molecular dynamics simulations. A simple model is proposed to describe the thermodynamic properties of alloys as a function of alloy composition. In particular, the

excess vibrational entropy of solid solution is calculated using the elastic constants of the system. Using this model, the polymorphic melting line $T_0(x)$ is determined. In alloys with fixed composition, the polymorphic melting temperature decreases as l decreases. Especially at l=0.85, $T_0(x)$ plunge sharply and crosses the glass transition line $T_g(x)$, which is a favorable condition for the glass formation according to the T_0 criterion of glass formation.

References

Baker, J.C., and Cahn, J.W. (1971). Thermodynamics of solidification. ASM, Metals Park: Ohio.

Blackman, M. (1951). On the Calculation of Characteristic Temperatures from the Elastic Constants. Philosophical Magazine *42*, 1441-1442.

Born, M.a.H., K. (1954). Dynamical theory of crystal lattices. Oxford University Press.

Cagin, T., and Ray, J.R. (1988a). Third-Order Elastic-Constants from Molecular-Dynamics - Theory and an Example Calculation. Phys. Rev. B *38*, 7940-7946.

Cagin, T., and Ray, J.R. (1988b). Elastic-Constants of Sodium from Molecular-Dynamics. Phys. Rev. B *37*, 699-705.

Cagin, T., and Ray, J.R. (1988c). Fundamental Treatment of Molecular-Dynamics Ensembles. Phys. Rev. A *37*, 247-251.

Cagin, T., and Ray, J.R. (1988d). Isothermal Molecular-Dynamics Ensembles. Phys. Rev. A *37*, 4510-4513.

Gordon, P. (1983). Principles of phase diagrams in materials systems. Krieger publishing company.

Hume-Rothery, W. (1969). The structure of metals and alloys. The institute of metals.

J. M. Prausnitz, R.N.L., and E. G. de Azevedo. (1986). Molecular thermodynamics of fluid-phase equilibria. Prentice-Hall Inc.

J. M. Smith, H.C.V.N. (1987). Introduction to chemical engineering thermodynamics.

Kauzmann, W. (1948). The Nature of the Glassy State and the Behavior of Liquids at Low Temperatures. Chem. Rev. *43*, 219-256.

Kittel, C. (1996). Introduction to solid state physics. John Wiley & Sons, Inc.

Luo, S.N., and Ahrens, T.J. (2003). Superheating systematics of crystalline solids. Appl. Phys. Lett. *82*, 1836-1838.

Massalski, T.B. (1981). The 4th international conference on rapidly quenched metals.

Mezard, M., and Parisi, G. (2000). Statistical physics of structural glasses. J. Phys.-Condes. Matter *12*, 6655-6673.

O. Kubaschewski, C.B.A., and P. J. Spencer. (1993). Materials thermo-chemistry. Pergamon press.

Peker, A. (1994). Formation and characterization of bulk metallic glasses, California Institute of Technology.

Rafiitabar, H., and Sutton, A.P. (1991). Long-Range Finnis-Sinclair Potentials for Fcc Metallic Alloys. Philos. Mag. Lett. *63*, 217-224.

Ray, J.R., and Rahman, A. (1985). Statistical Ensembles and Molecular-Dynamics Studies of Anisotropic Solids .2. J. Chem. Phys. *82*, 4243-4247.

Reif, F. (1985). Fundamentals of statistical and thermal physics. McGraw-Hill.

Siethoff, H., and Ahlborn, K. (1995). The Dependence of the Debye Temperature on the Elastic Constants. Phys. Status Solidi B-Basic Res. *190*, 179-191.

Sommer, F., Singh, R.N., and Witusiewicz, V. (2001). On the entropy of mixing. J. Alloy. Compd. *325*, 118-128.

Sutton, A.P., and Chen, J. (1990). Long-Range Finnis Sinclair Potentials. Philos. Mag. Lett. *61*, 139-146.

Swalin, R.A. (1972). Thermodynamics of solids. A Wiley-Interscience Publication.

Turnbull, D. (1950). J. Appl. Phys. *21*, 1022.

Ziman, J.M. (1972). Principles of the theory of solids. Cambridge university press.

Table 2-1. Atom size parameters for the Sutton-Chen (SC) many-body potential. Other parameters, such as *e*, *c*, *m*, and *n*, are kept the same as in Table 1-1. The parameter l is defined as the size ratio of Cu^{*} to Cu^{**}. These size parameters were chosen to keep constant the geometric mean of the size parameters for Cu^{*} and Cu^{**}, $a_{ij} = \sqrt{a_{ii} a_{jj}}$.

λ	a of Cu^{*}	a of Cu^{**}
0.85	3.32180	3.90800
0.90	3.41811	3.79790
0.95	3.51177	3.69660

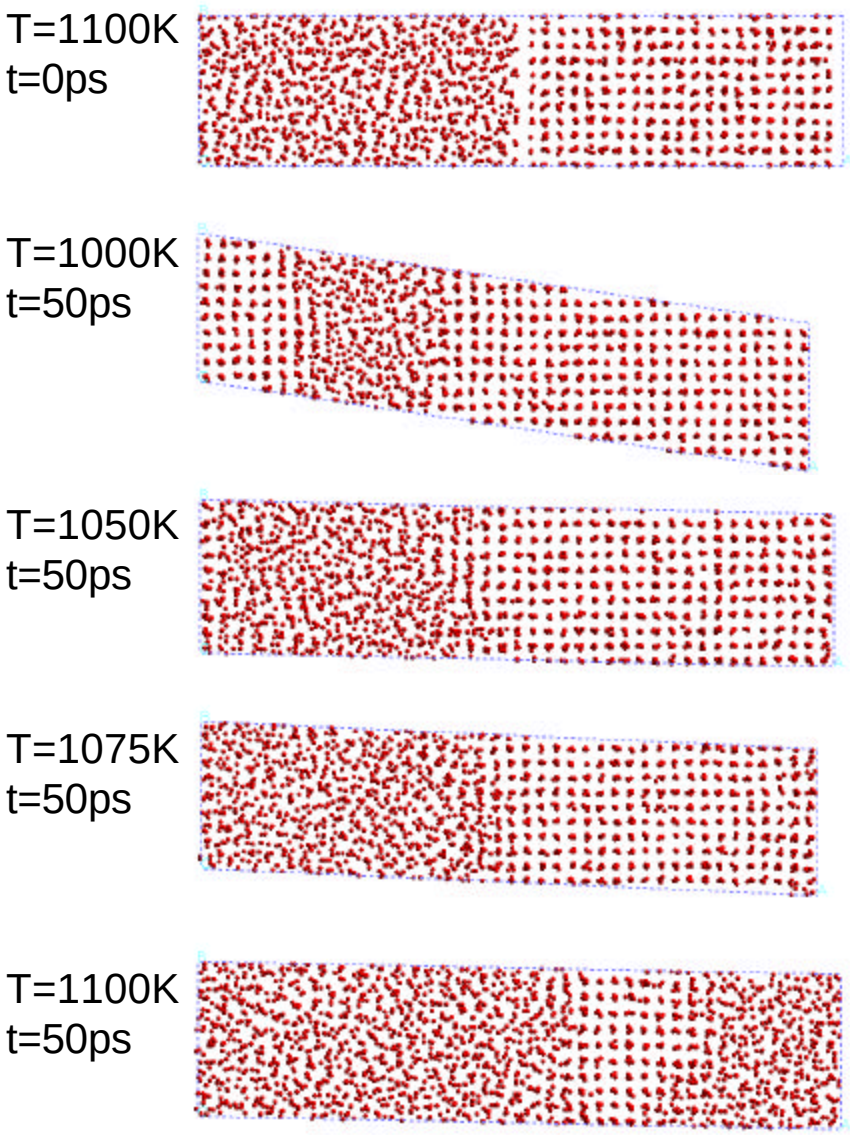

Figure 2-1(a). Snapshots of the two phase simulations are shown. At each temperature, the initial structure (t=0) is prepared by putting the equilibrium liquid and crystal together in one unit cell (top figure). If $T<T_m$, the crystal phase grows. If $T>T_m$, the liquid phase grows. If $T=T_m$, the two phases remain at equilibrium.

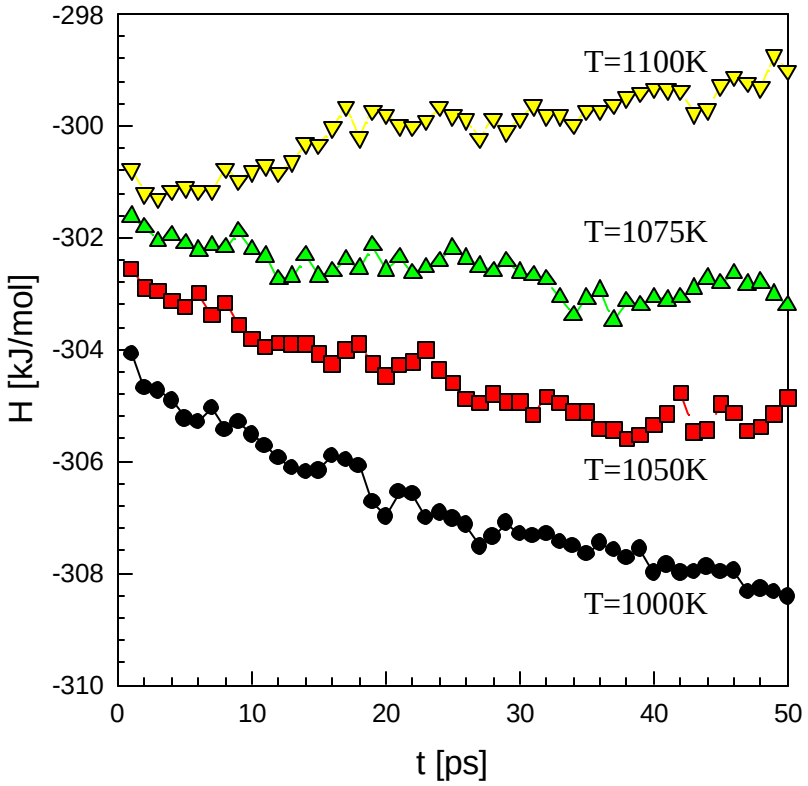

Figure 2-1(b). The enthalpy H of the two phase simulation as a function of time t at different temperatures. If $T>T_m$, the crystalline phase melts, therefore, H increases because of the heat of fusion. If $T<T_m$, the liquid phase crystallizes, therefore, H decreases. From this, the melting temperature is estimated to be 1075K$<T_m<$1100K.

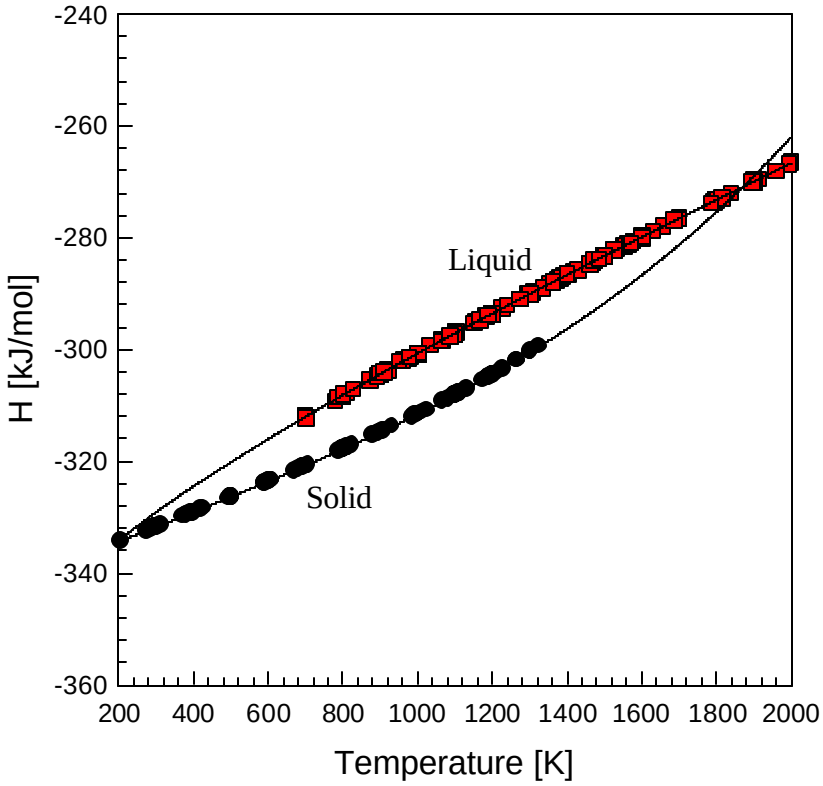

Figure 2-2. The enthalpy of pure metal (solid and liquid states) as a function of temperature of the solid and liquid phases. Due to the fast heating/cooling rate (4×10^{12} K/s) and PBC (no surface effects), the system tends to be easily superheated/supercooled. Therefore, MD can provide the thermodynamic data in a broad temperature range thus makes the use of Eq. 2-2 more accurate. The lines are fit to the data using Eq. 2-2.

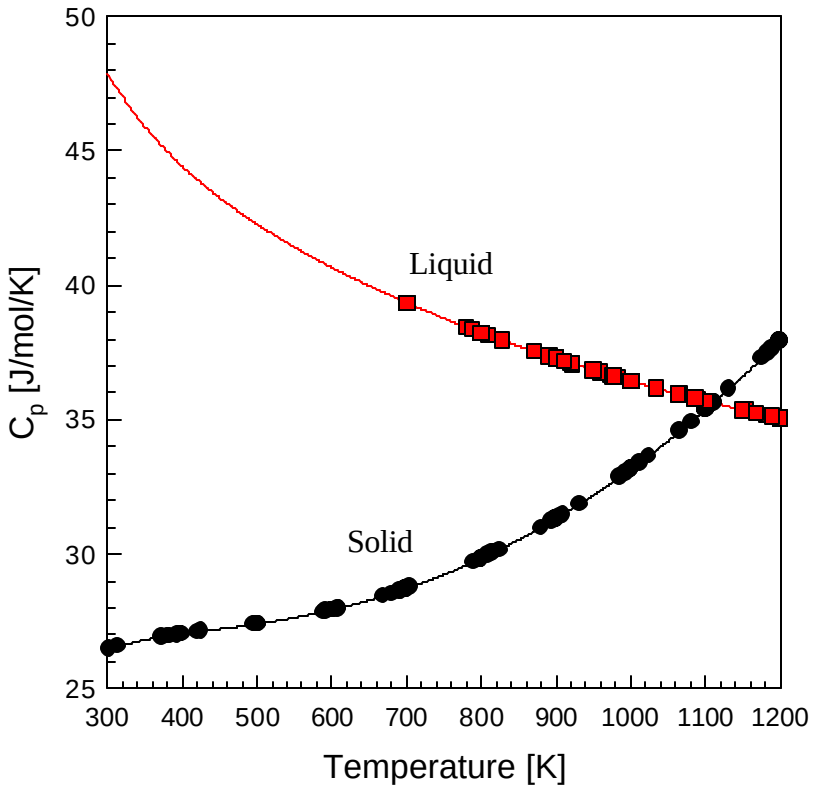

Figure 2-3. The heat capacity C_p of pure metal (solid and liquid states) as a function of temperature. The lines are fit to the data using Eq. 2-1.

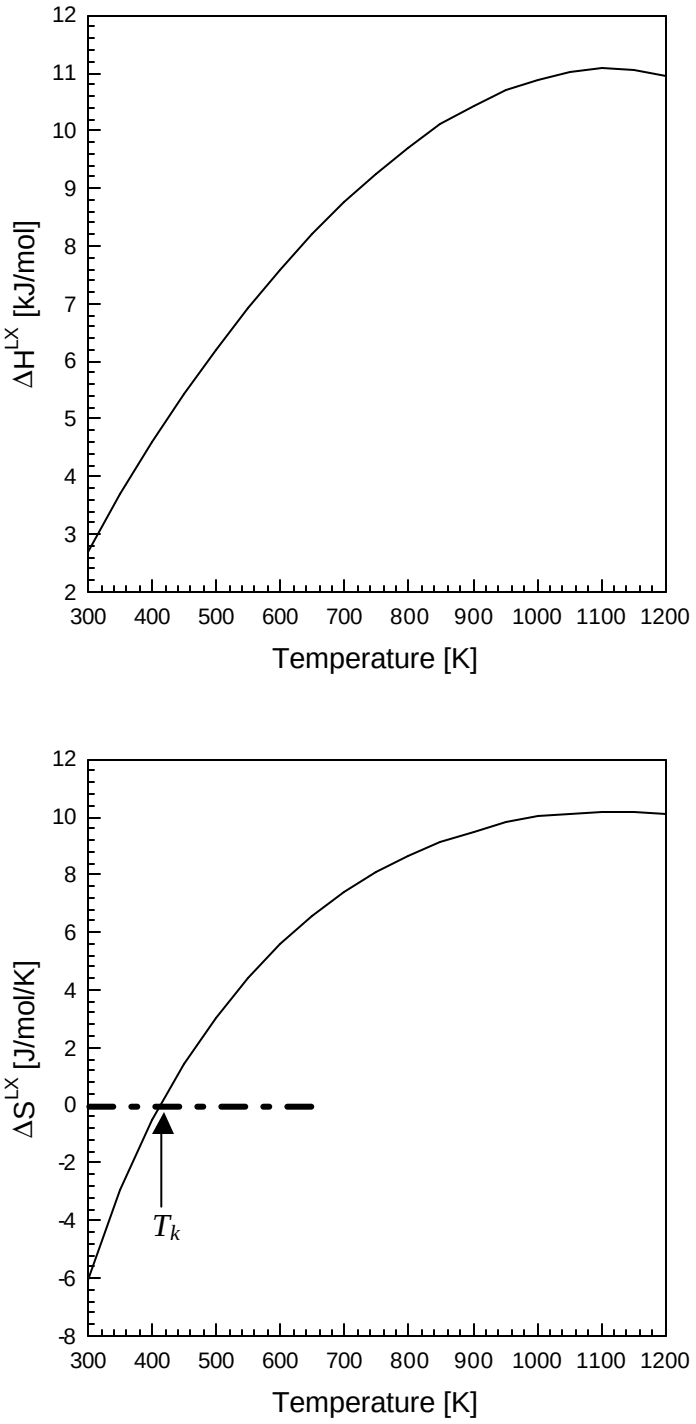

Figure 2-4. The enthalpy (top) and entropy (bottom) differences between the liquid and solid states of pure metal as a function of temperature.

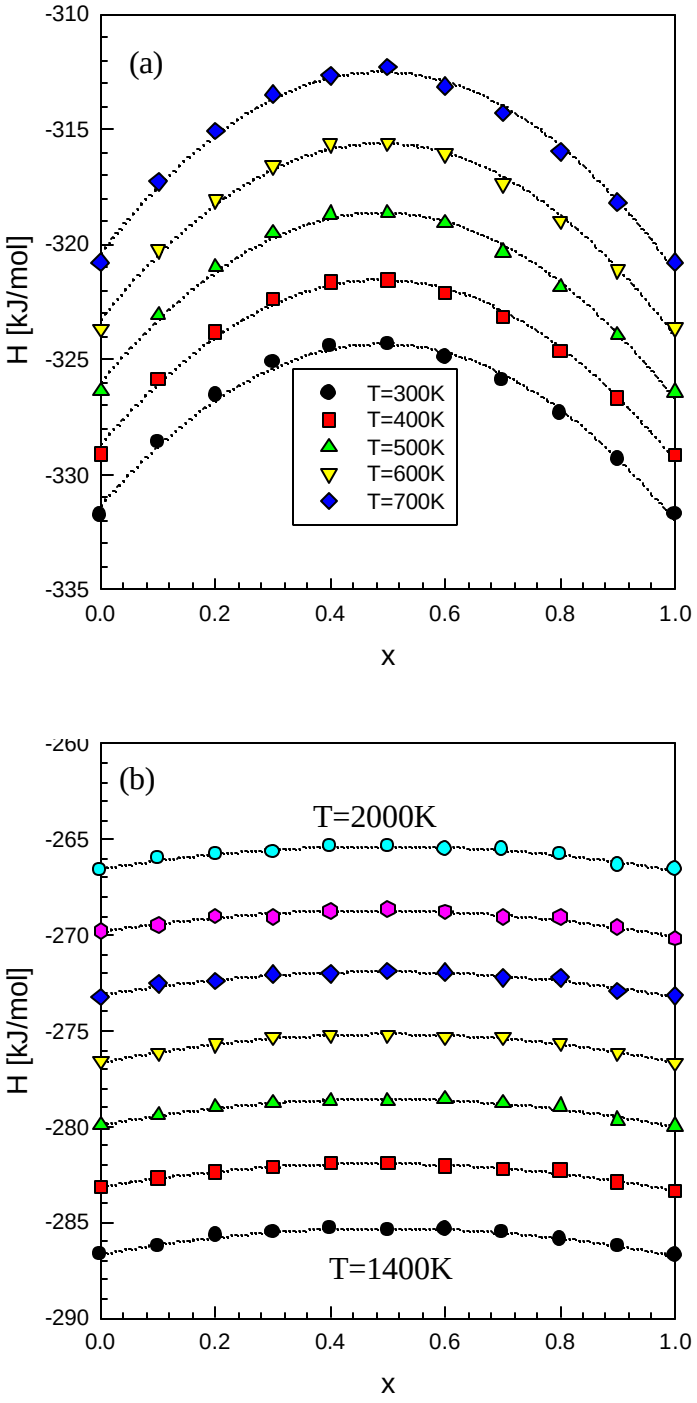

Figure 2-5. The enthalpy H of the solid (top) and the liquid (bottom) as a function of concentration x at different temperatures. The temperature interval is 100K and the lines are fit to the parabolic equation $y(x) = \Omega x(1-x)$ (Eq. 2-8).

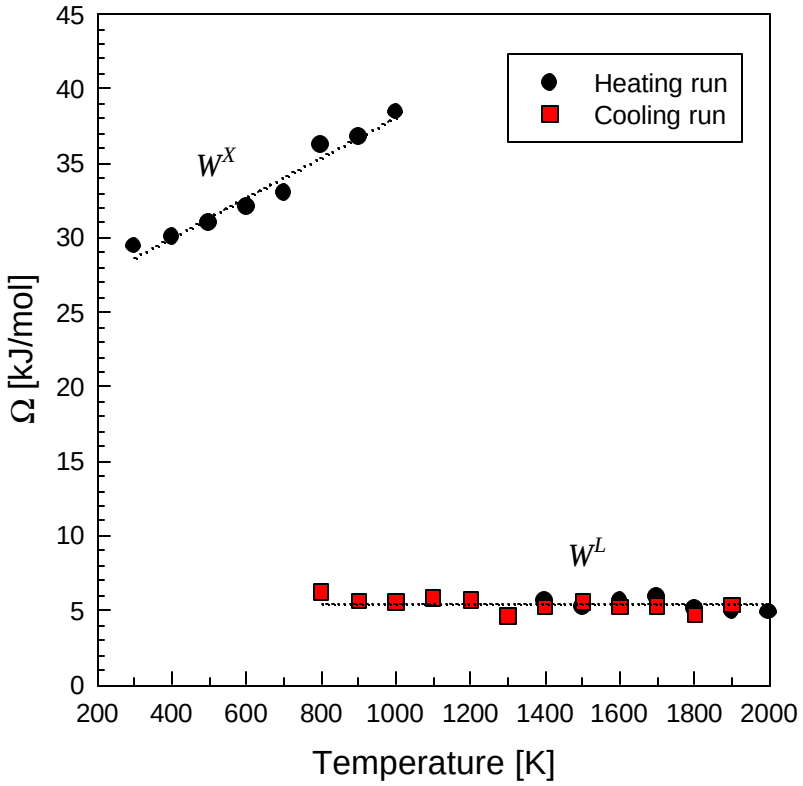

Figure 2-6. Ω^X and Ω^L as a function of temperature at l=0.85. Ω^X is fitted to $y(x) = a^X T + b^X$, where a^X=0.0134455kJ/mol/K and b^X=24.6167kJ/mol. Ω^L is fitted to y=5.38938 kJ/mol.

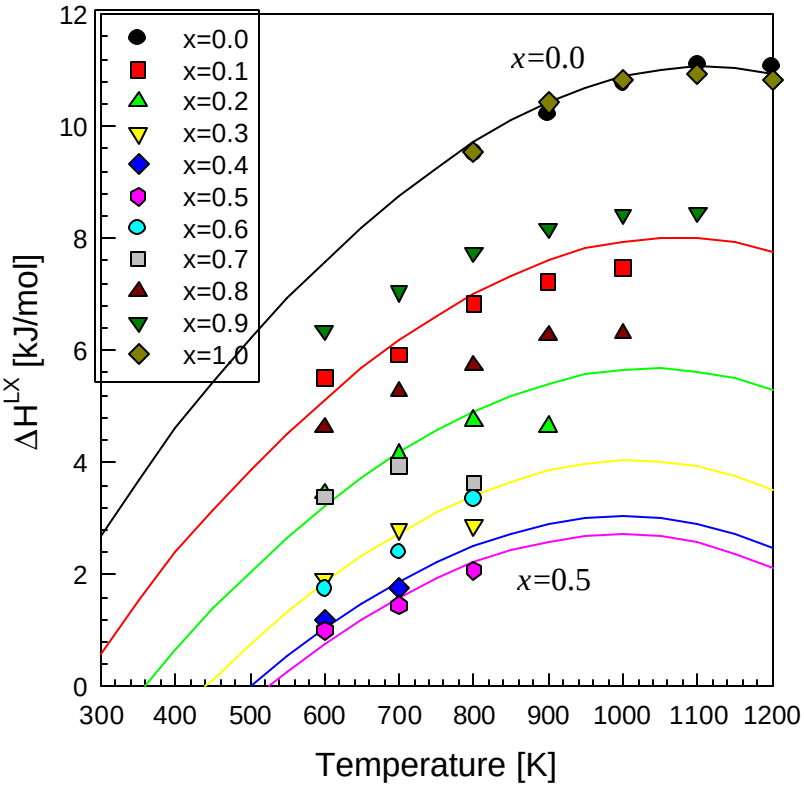

Figure 2-7. The enthalpy difference between the liquid and solid phases ΔH^{LX} as a function of temperature for the concentrations x=0, 0.1, 0.2, 0.3, 0.4, and 0.5. The symbols are data points obtained directly from MD and the lines are from Eq. 2-12.

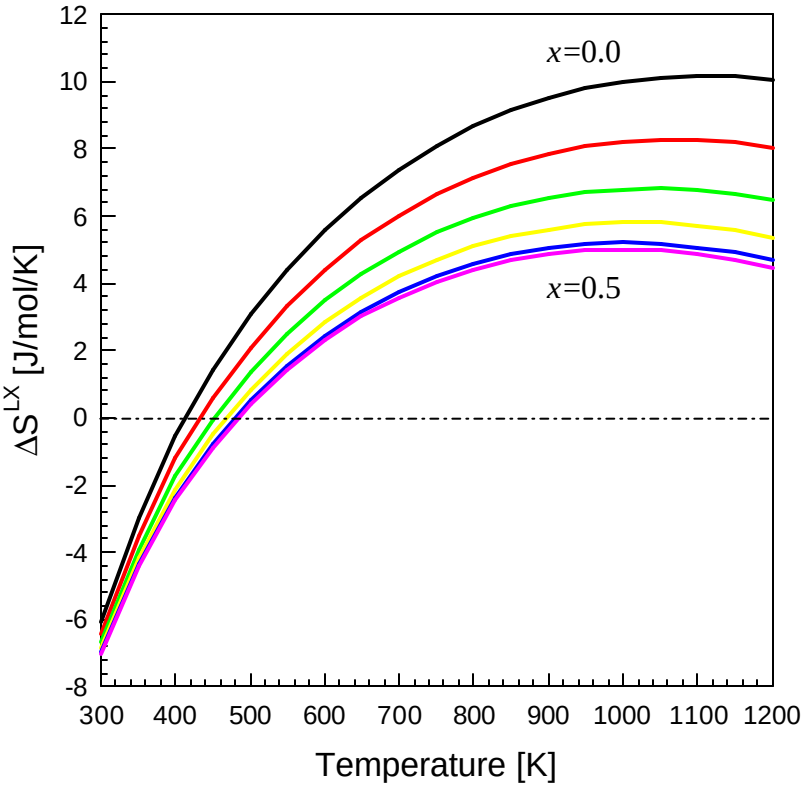

Figure 2-8. The entropy difference between the liquid and solid phases ΔS^{LX} as a function of temperature for the concentrations (from top to bottom) x=0, 0.1, 0.2, 0.3, 0.4, and 0.5.

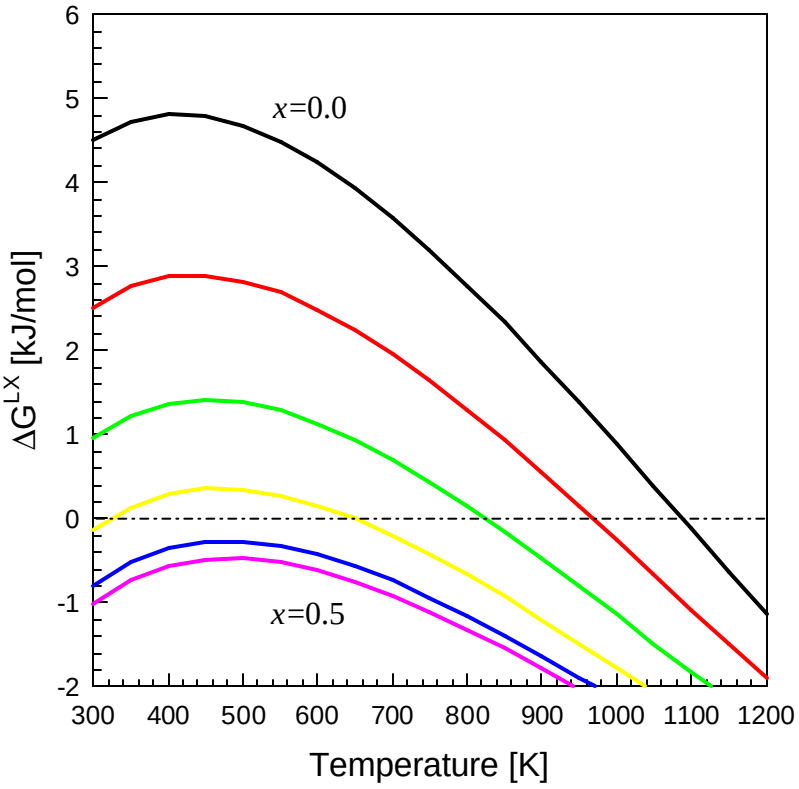

Figure 2-9. The Gibbs free energy difference between the liquid and solid phases ΔG^{LX} as a function of temperature for the concentrations (from top to bottom) x=0, 0.1, 0.2, 0.3, 0.4, and 0.5.

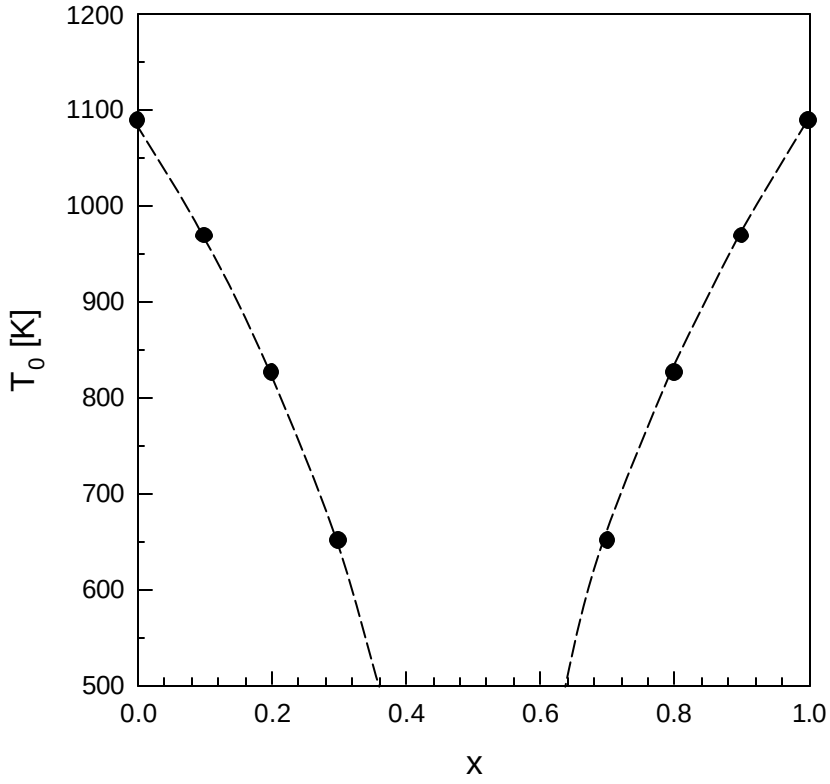

Figure 2-10. The polymorphic melting line $T_0(x)$ as a function of concentration x.

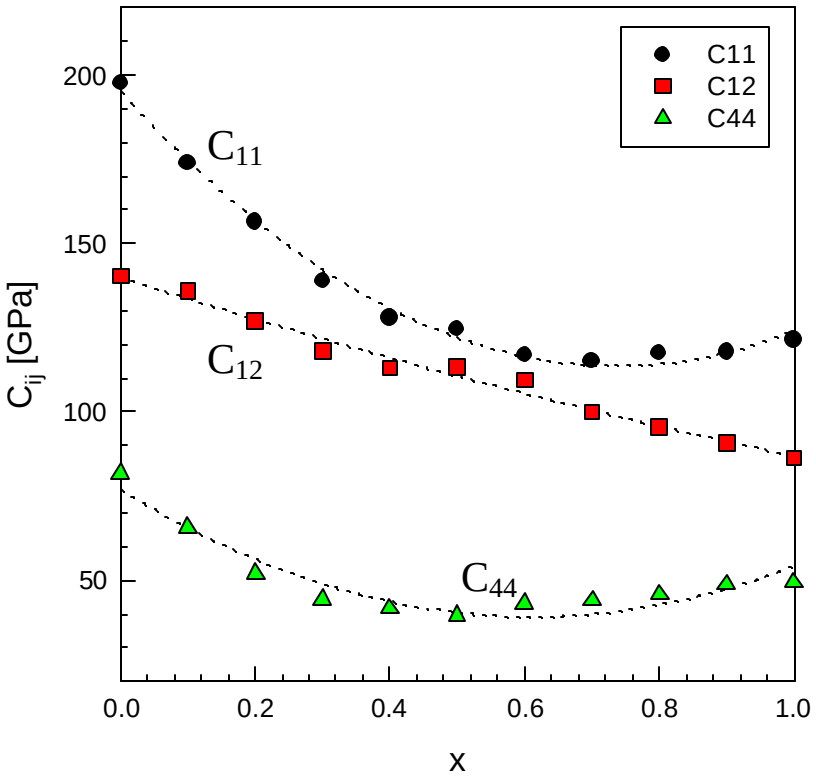

Figure 2-11. The elastic constants for the $Cu^{*}_{1-x}Cu^{**}_{x}$ system at T=300K. The size ratio of Cu^{*} to Cu^{**} is 0.85. The dotted lines are drawn empirically as a guide.

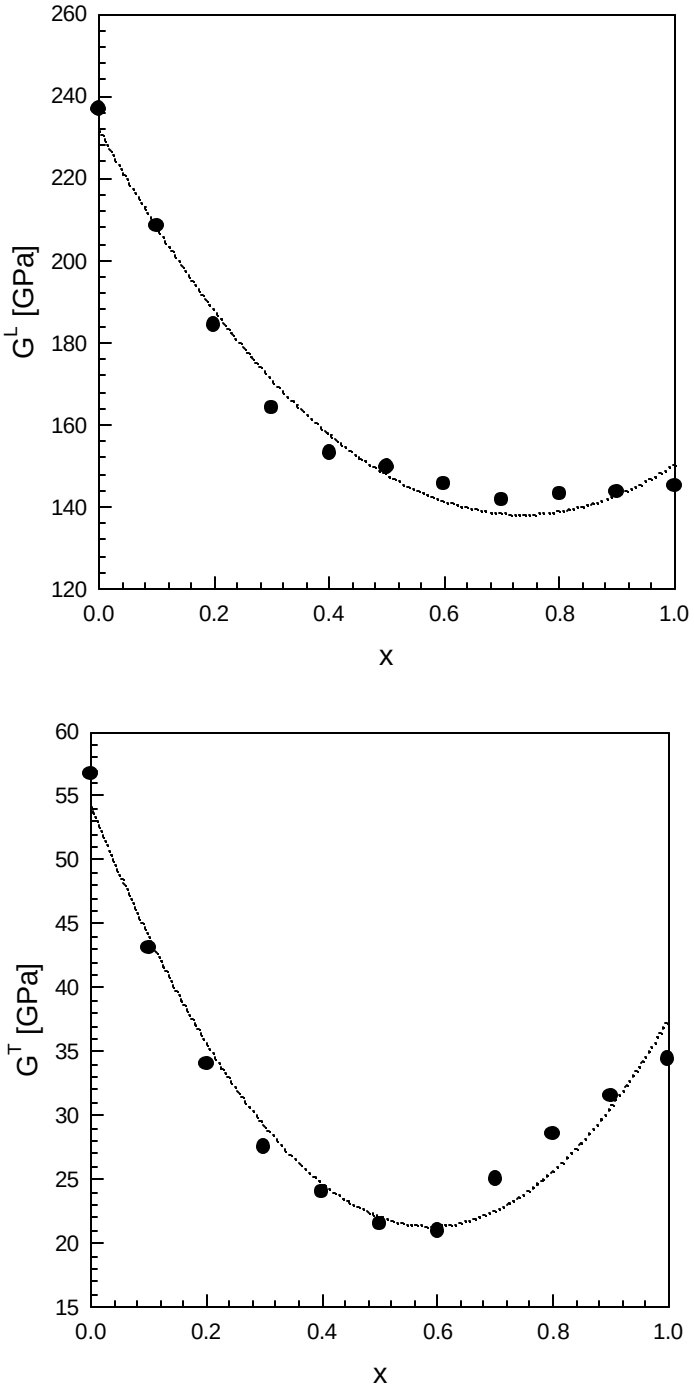

Figure 2-12. The effective elastic constants in the longitudinal mode G^L (top) and the transverse mode G^T (bottom) as a function of concentration x. The dotted lines are drawn empirically as a guide.

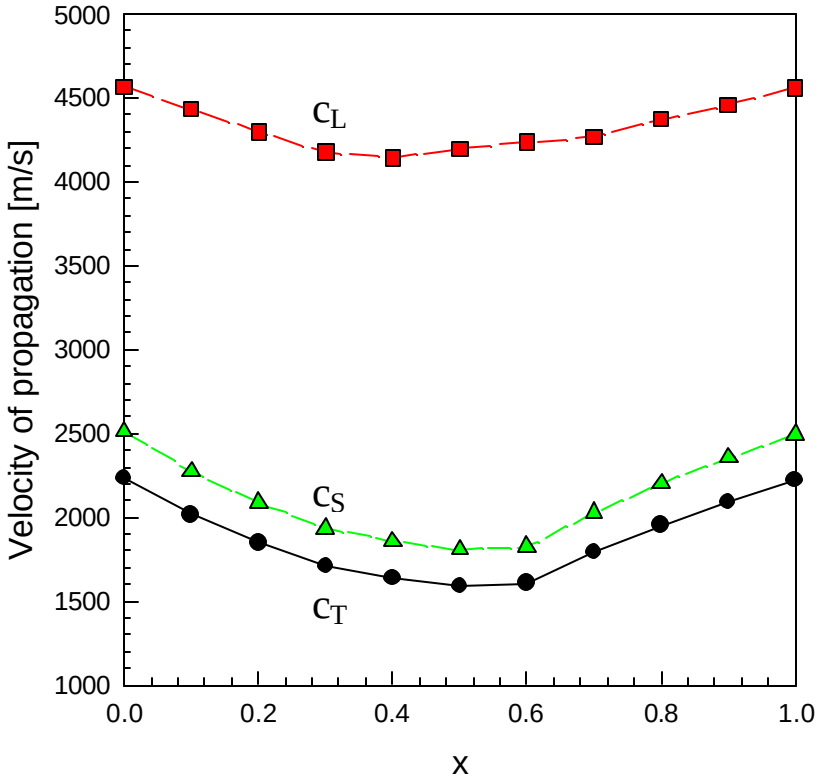

Figure 2-13. The velocity of propagation as a function of Cu^{**} concentration x. Here, c_L and c_T are the velocities of propagation in the longitudinal and transverse directions, respectively. c_S is the effective sound velocity as defined by Eq. 2-22.

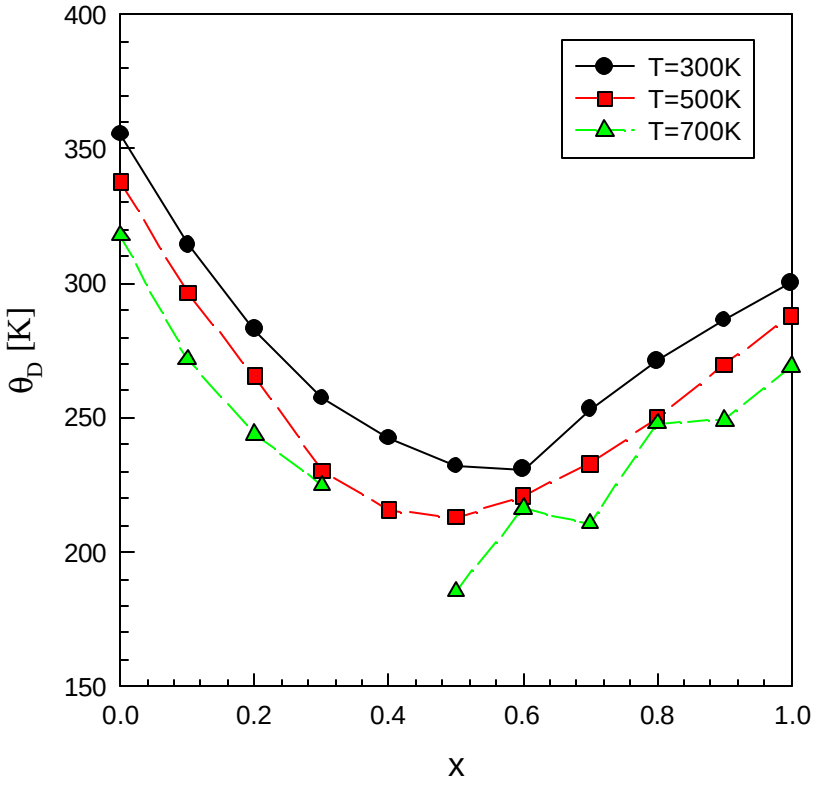

Figure 2-14. The Debye temperature as a function of Cu** concentration *x* calculated from the elastic constants at different temperatures. At T=700K and *x*=0.4, the effective elastic constant in the transverse mode becomes negative, resulting in a non-physical q_D.

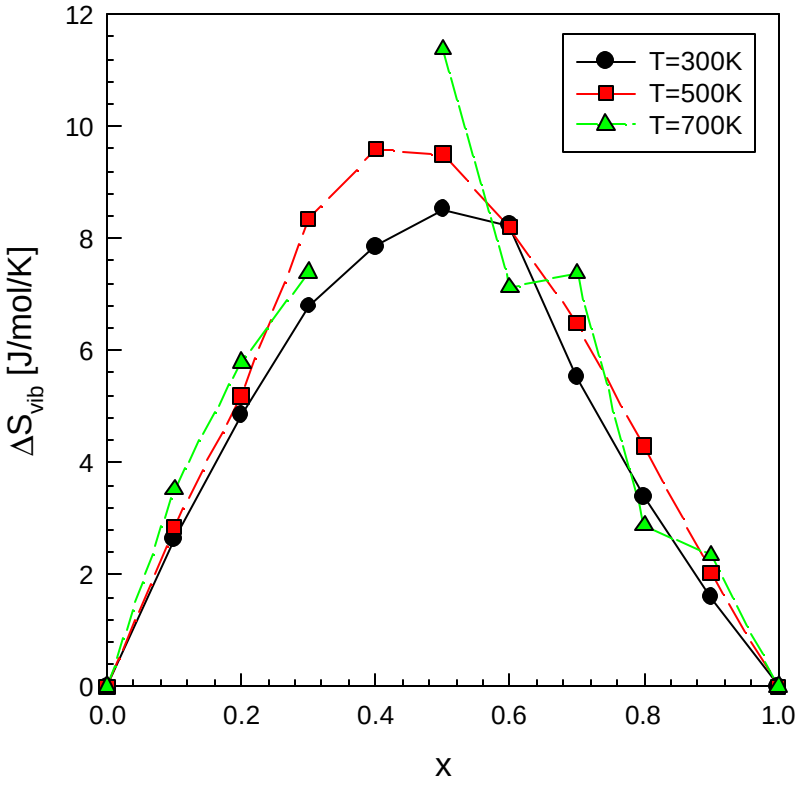

Figure 2-15. The excess vibrational entropy ΔS^{vib} as a function of Cu^{**} concentration x calculated using the elastic constants. The data point at T=700K and x=0.4 is omitted because the effective elastic constant in the transverse mode becomes negative.

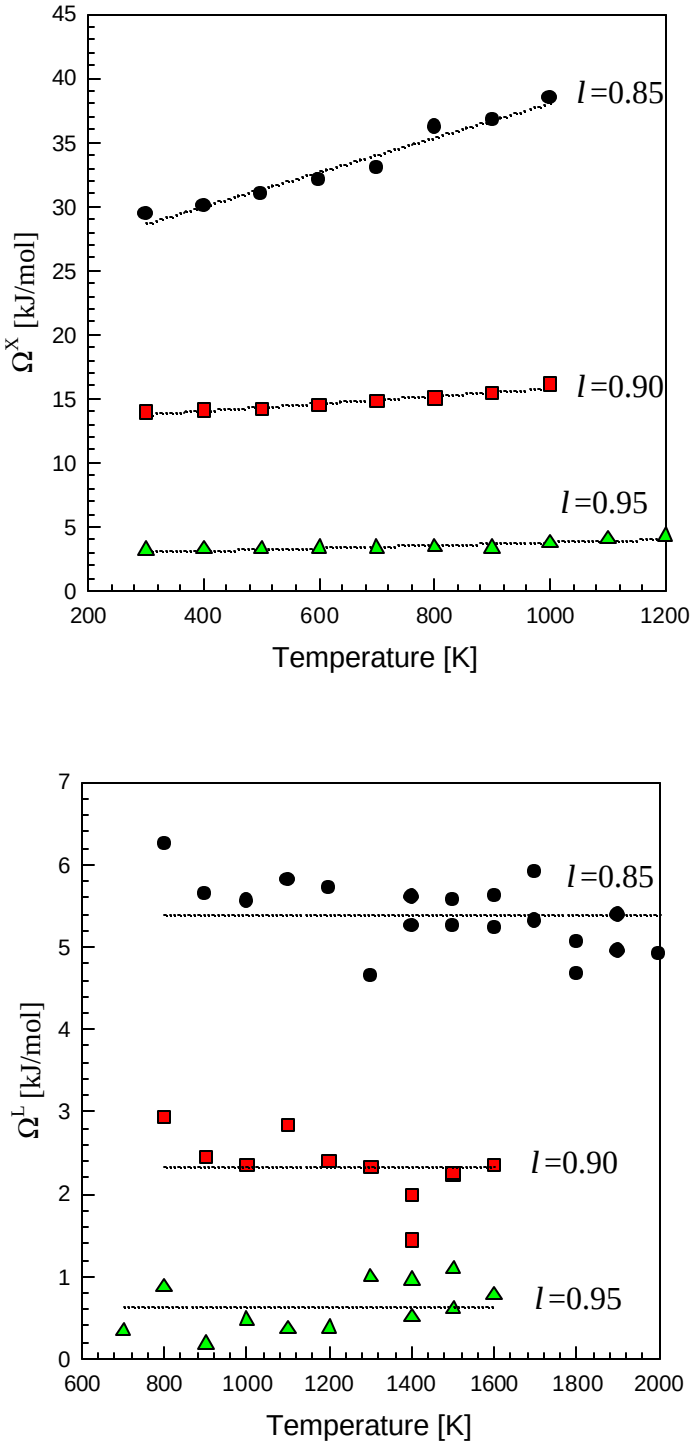

Figure 2-16. Ω^X (top) and Ω^L (bottom) as a function of temperature at different size ratio l. Ω^X is fitted to $y(x) = a^X T + b^X$ while Ω^L is fitted to y=constant.

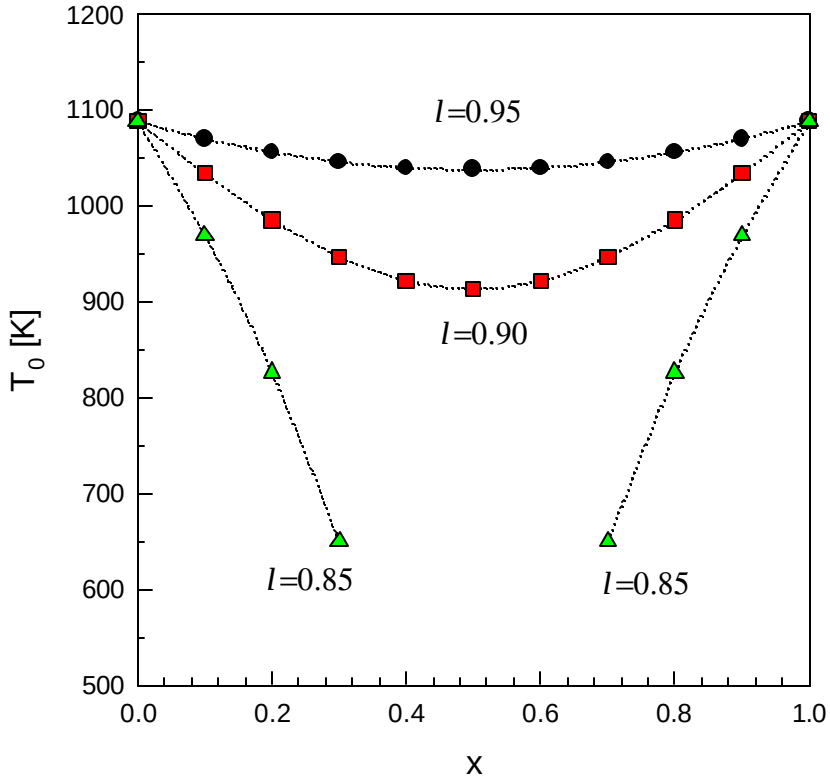

Figure 2-17. The polymorphic melting line $T_0(x)$ as a function of concentration x for different l.

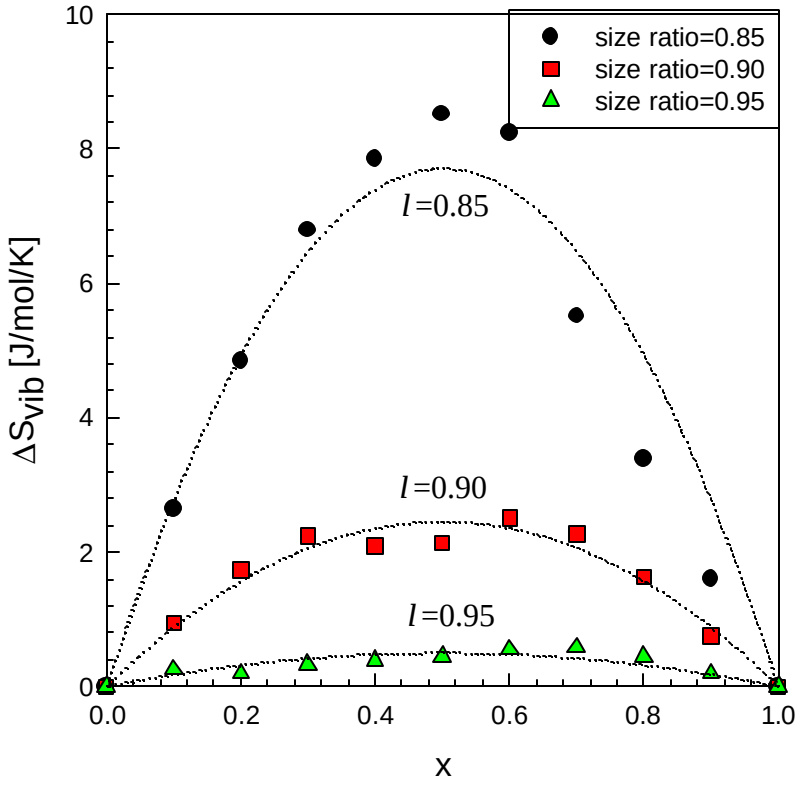

Figure 2-18. The vibrational entropy of mixing ΔS^{vib} as a function of Cu^{**} concentration x for different size ratio l. The data are fitted to the parabolic equation $y(x) = hx(1-x)$ (dotted lines). Corresponding h values are 29.43 for l=0.85, 13.98 for l=0.90, and 3.17 for l=0.95 in units of J/mol/K.

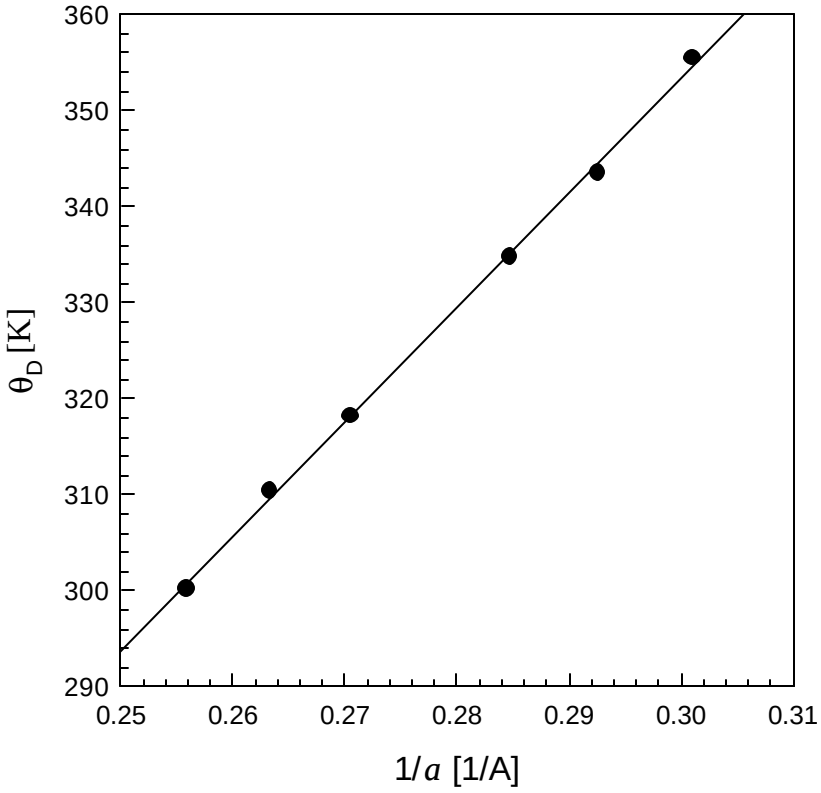

Figure 2-19. The Debye temperature versus inverse of the lattice constant in pure metals. The line is $y(x)$=1193.5748x-4.7352, where correlation constant R^2=0.9987.